

Variational identification of minimal seeds to trigger transition in plane Couette flow

S. M. E. RABIN¹†, C. P. CAULFIELD^{2,1}
AND R. R. KERSWELL³

¹Department of Applied Mathematics & Theoretical Physics, Centre for Mathematical Sciences, University of Cambridge, Wilberforce Road, Cambridge CB3 0WA, UK

²BP Institute, University of Cambridge, Madingley Rise, Madingley Road, Cambridge CB3 0EZ, UK

³School of Mathematics, University of Bristol, BS8 1TW Bristol, UK

(Received 1 November 2018)

A variational formulation incorporating the full Navier-Stokes equations is used to identify initial perturbations with finite kinetic energy E_0 which generate the largest gain in perturbation kinetic energy (across all possible time intervals) for plane Couette flow. Two different representative flow geometries are chosen corresponding to those used previously by Butler & Farrell (1992) and Monokrousos *et al.* (2011). In the former (smaller geometry) case as E_0 increases from 0, we find an optimal which is a smooth nonlinear continuation of the well-known linear result at $E_0 = 0$. At $E_0 = E_c$, however, completely unrelated states are uncovered which trigger turbulence and our algorithm consequently fails to converge. As $E_0 \rightarrow E_c^+$, we find good evidence that the turbulence-triggering initial conditions approach a ‘minimal seed’ which corresponds to the state of lowest energy on the laminar-turbulent basin boundary or ‘edge’. This situation is repeated in the Monokrousos *et al.* (2011) (larger) geometry albeit with one notable new feature - the appearance of a nonlinear optimal (as found recently in pipe flow by Pringle & Kerswell (2010) and boundary layer flow by Cherubini *et al.* (2010)) at finite $E_0 < E_c$ which has a very different structure to the linear optimal. Again the minimal seed at $E_0 = E_c$ does not resemble the linear or now the nonlinear optimal. Our results support the first of two conjectures recently posed by Pringle *et al.* (2011) but contradict the second. Importantly, their prediction that the form of the functional optimised is not important for identifying E_c providing heightened values are produced by turbulent flows is confirmed: we find the what looks to be the same E_c and minimal seed using energy gain as opposed to total dissipation in the Monokrousos *et al.* (2011) geometry.

1. Introduction

The investigation of hydrodynamic stability is one of the canonical problems of fluid dynamics. A particularly interesting archetypal flow is plane Couette flow (PCF), where the flow is between two parallel plates moving at a relative velocity $2U$, separated by a distance $2h$, with thus a characteristic Reynolds number $Re = Uh/\nu$ where ν is the kinematic viscosity. PCF is linearly stable for even large Re (Romanov (1973)) yet turbulence has been observed experimentally as low as $Re = 325$ (Bottin & Chate (1998)). It has been hypothesized that transient perturbation growth, due to the non-normality of the underlying linear operator of the Navier-Stokes equations, may explain this disconnect. Several authors (for example Gustavsson (1991); Butler & Farrell (1992);

† Email address for correspondence: s.rabin@damtp.cam.ac.uk

Reddy & Henningson (1993)) demonstrated that substantial transient kinetic energy gain $G(T) = E(T)/E(0)$ (where $E(T)$ is the infinitesimally small kinetic energy at the final time T) could be achieved by a linear (infinitesimal) optimal perturbation (LOP) (see Schmid (2007) for a review). Proponents of such an essentially linear mechanism for energy growth point to the Reynolds-Orr equation (Schmid (2007)) as an indication that energy growth is a linear effect, as this equation shows that dE/dt is independent of the nonlinear advective terms in the Navier–Stokes equations. The argument is that if a real flow is seeded with a ‘small’, yet finite amplitude perturbation with the same structure as a LOP, the transient energy gain of the LOP could be sufficiently large to ‘push’ the perturbation into the ‘nonlinear regime’ and hence trigger transition.

However, this line of thinking is based on a couple of implicit assumptions: that the ‘entrance’ into the nonlinear regime of this perturbation will lead to turbulence; and that the linear optimal perturbation (LOP) is still the ‘best’ choice for the growth of nonlinear perturbations. The latter assumption can be explicitly probed by posing the optimal growth problem for initial perturbations of finite amplitude which can affect the base flow as they grow. This has been done recently for pipe flow (Pringle & Kerswell (2010)) and boundary layer flow (Cherubini *et al.* (2010)) with both studies discovering the existence of a nonlinear optimal perturbation (NLOP) which has a very different structure to the LOP and outgrows it beyond a small but finite energy threshold.

With more of an eye on reaching turbulence, Monokrousos *et al.* (2011) posed a different problem for PCF by maximising the total energy dissipation over a long but fixed time period. They purposely looked for a turbulent end state at the end of their optimisation window and then worked downwards in initial energy to identify the threshold for transition. Earlier, Pringle & Kerswell (2010) had failed to identify this threshold by working upwards in initial energy because of convergence issues. However, a follow-up study (Pringle *et al.* (2011), henceforth referred to as PWK11) with a more efficient code run at higher resolution succeeded in identifying a (converged) nonlinear optimal for larger initial energies. At $E_0 = E_{fail}$, they again found a failure to converge but noticed that this corresponded to their optimisation algorithm encountering turbulent (end) flows. The conclusion was that this failure energy E_{fail} is sufficiently large to enable an initial perturbation to undergo the transition to turbulence: i.e. $E_{fail} \geq E_c$, the energy threshold of transition (PWK11 actually conjectured that $E_{fail} = E_c$: see Conjecture 1 below). In dynamical systems parlance, this initial perturbation is then in the basin of attraction of the turbulence or more generally (if the turbulence is actually not an attractor but a chaotic saddle), has crossed the ‘edge’, a hypersurface which separates initial conditions which become turbulent from those which relaminarise (Itano & Toh (2001); Skufca *et al.* (2006); Schneider *et al.* (2007); Duguet *et al.* (2008)). The picture then put forward by PWK11 is that as E_0 increases from 0, the $E = E_0$ hypersurface in phase space intersects the edge for the first time at $E_0 = E_c$ and that the initial perturbation which corresponds to their (generically unique) intersection at $E_0 = E_c$ is the ‘minimal seed’ for triggering turbulence. This seed is ‘minimal’ in the sense that it is the lowest energy state on the edge and therefore represents the most energy efficient way of triggering turbulence by adding an infinitesimal perturbation to it. PWK11 also find evidence to suggest that the NLOP tends to the minimal seed associated with this loss of convergence (and transition to turbulence) as $E_0 \rightarrow E_c^-$. They summarise their thinking as two conjectures.

“ **Conjecture 1:** For T sufficiently large, the initial energy value E_{fail} at which the energy growth problem first fails (as E_0 is increased) to have a smooth optimal solution will correspond exactly to E_c .

Conjecture 2: For T sufficiently large, the optimal initial condition for maximal en-

ergy growth at $E_0 = E_c - \epsilon^2$ converges to the minimal seed at E_c as $\epsilon \rightarrow 0$. ”

In this paper, we wish to investigate the validity of these conjectures in the context of PCF. Two sets of geometry and Reynolds numbers are considered for PCF, one discussed in each of Butler & Farrell (1992) (henceforth referred to as BF92) - a relatively narrow spanwise domain with $Re = 1000$ - and Monokrousos *et al.* (2011) (henceforth referred to as M11) who used a domain with double the spanwise extent at $Re = 1500$. By considering these different situations, we are able to investigate whether there is anything generic that can be said about the progression of optimal perturbations starting with the (infinitesimal) LOPs at $E_0 = 0$, through NLOPs as E_0 increases to the minimal seed at $E_0 = E_c$. Of principal interest will be whether this approach can identify E_c and the form of the minimal seed either directly (by smooth evolution of the optimal as $E_0 \rightarrow E_c^-$) or indirectly (by failing to converge). By considering the M11 geometry but choosing to maximise the energy gain rather than total energy dissipation, we also assess the sensitivity of the procedure to the exact choice of optimising functional.

From the technical perspective, we also take this opportunity to further develop the variational formulation to include optimisation over T , the duration of the observation window or ‘target time’. This means we are then able to identify the initial perturbation which achieves the highest gain possible over *all* T with the corresponding optimal final time now an interesting output. All previous studies (Pringle & Kerswell (2010); Pringle *et al.* (2011); Cherubini *et al.* (2010); Monokrousos *et al.* (2011)) chose to work with a pre-defined T over which to perform their optimization. Conceptually, letting T be an output of the optimisation seems a significant advance yet operationally, it requires only a small adjustment in the algorithm.

The plan of the paper is as follows. In section 2 we briefly present the variational framework and discuss how the new target time optimisation is carried out. The following two sections, 3 and 4, discuss the results obtained for the BF92 and M11 situations respectively. A final section 5 then discusses the results in light of the above-quoted conjectures of PWK11 and draws a number of conclusions.

2. Lagrangian framework

We seek the initial disturbance of kinetic energy E_0 to the laminar flow which attains the largest energy growth $G(T) := E(T)/E_0$ a time T later while evolving under the Navier-Stokes equations, remaining incompressible and respecting the applied boundary conditions. Here $E(T) := \frac{1}{2} \langle \mathbf{u}(T), \mathbf{u}(T) \rangle$, with the angle brackets denoting,

$$\langle \mathbf{v}, \mathbf{u} \rangle := \frac{1}{V} \int_{\mathcal{D}} \mathbf{v}^\dagger \mathbf{u} \, dV, \quad (2.1)$$

where \dagger denotes the Hermitian conjugate, and V is the volume of the domain \mathcal{D} . The flow configuration considered is PCF with coordinate system such that the streamwise direction is x , the wall normal direction is y and the spanwise direction z . The x and z directions are assumed to be periodic and the separation between the walls ($2h$) is used to scale length so that their positions are given by $y = \pm 1$. The speed difference between the walls ($2U$) scales the velocity so that the non-dimensionalised background Couette flow is $\mathbf{U}(y) = y\mathbf{e}_x$ and the Reynolds number $Re := Uh/\nu$.

The functional to be extremised is the energy gain which, when constrained by the Navier Stokes equations, the initial energy value $E(0) = E_0$ and incompressibility, pro-

duces the Lagrangian

$$\mathcal{L} := \frac{E(T)}{E_0} - [\partial_t \mathbf{u} + N(\mathbf{u}) + \nabla p, \mathbf{v}] - [\nabla \cdot \mathbf{u}, q] - \left(\frac{1}{2} \langle \mathbf{u}_0, \mathbf{u}_0 \rangle - E_0 \right) c + \langle \mathbf{u}_0 - \mathbf{u}(0), \mathbf{v}_0 \rangle. \quad (2.2a)$$

N is the nonlinear operator

$$N(u_i) := U_j \partial_j u_i + u_i \partial_i U_j + u_j \partial_j u_i - \frac{1}{Re} \partial_j \partial_j u_i, \quad (2.2b)$$

and square brackets denote a time average of the inner product,

$$[\mathbf{v}, \mathbf{u}] := \frac{1}{T} \int_0^T \langle \mathbf{v}, \mathbf{u} \rangle dt. \quad (2.3)$$

In the Lagrangian, \mathbf{v} , q , \mathbf{v}_0 and c are Lagrange multipliers, \mathbf{u}_0 is the initial value of the perturbation velocity \mathbf{u} and \mathbf{U} the background Couette flow. While not strictly necessary to divide our cost functional by E_0 we found it easier to tune our algorithm by doing so.

Taking first variations of the Lagrangian with respect to \mathbf{v} , q , \mathbf{v}_0 and c and setting them to zero recovers (respectively) the constraints of the Navier Stokes equations, incompressibility, the initial kinetic energy of E_0 and initial state $\mathbf{u}_0 = \mathbf{u}(0)$,

$$\frac{\delta \mathcal{L}}{\delta \mathbf{v}} = \partial_t \mathbf{u} + N(\mathbf{u}) + \nabla p := 0, \quad (2.4)$$

$$\frac{\delta \mathcal{L}}{\delta q} = \nabla \cdot \mathbf{u} := 0, \quad (2.5)$$

$$\frac{\delta \mathcal{L}}{\delta \mathbf{v}_0} = \mathbf{u}_0 - \mathbf{u}(0) := 0. \quad (2.6)$$

$$\frac{\delta \mathcal{L}}{\delta c} = \frac{1}{2} \langle \mathbf{u}_0, \mathbf{u}_0 \rangle - E_0 := 0. \quad (2.7)$$

First variations with respect to the physical variables yields a complementary set of adjoint equations,

$$\frac{\delta \mathcal{L}}{\delta \mathbf{u}} = \partial_t \mathbf{v} + N^\dagger(\mathbf{v}, \mathbf{u}) + \nabla q + \left(\frac{\mathbf{u}}{E_0} - \mathbf{v} \right) \Big|_{t=T} + (\mathbf{v} - \mathbf{v}_0) \Big|_{t=0} := 0, \quad (2.8)$$

$$\frac{\delta \mathcal{L}}{\delta p} = \nabla \cdot \mathbf{v} := 0, \quad (2.9)$$

$$\frac{\delta \mathcal{L}}{\delta \mathbf{u}_0} = \mathbf{v}_0 - c \mathbf{u}_0 := 0. \quad (2.10)$$

Here,

$$N^\dagger(v_i, \mathbf{u}) := \partial_j (u_j v_i) - v_j \partial_i u_j + \partial_j (U_j v_i) - v_j \partial_i U_j + \frac{1}{Re} \partial_j \partial_j v_i \quad (2.11)$$

can be identified as the adjoint of N and \mathbf{v} , \mathbf{v}_0 and q are the adjoint variables of \mathbf{u} , \mathbf{u}_0 and p . Equation (2.8) is in reality three equations. The first part, $\partial_t \mathbf{v} + N^\dagger(\mathbf{v}, \mathbf{u}) + \nabla q = \mathbf{0}$, must be satisfied at all times and is the adjoint Navier Stokes equation. Since the full Navier-Stokes equations have been imposed, the adjoint operator depends on the velocity field \mathbf{u} . The sign of the diffusion term is also reversed and therefore the adjoint equation can only be solved backwards in time. The second part of (2.8), $(\mathbf{u}/E_0 - \mathbf{v}) \Big|_{t=T} = \mathbf{0}$, is a terminal condition, linking our physical and adjoint variables and needs only to be satisfied at time T . The third part, $(\mathbf{v} - \mathbf{v}_0) \Big|_{t=0} = \mathbf{0}$, is a condition linking \mathbf{v}_0 and $\mathbf{v}(0)$, which must be satisfied at $t = 0$.

Further to previous recent formulations (Pringle & Kerswell (2010); Pringle *et al.* (2011);

(Cherubini *et al.* (2010); Monokrousos *et al.* (2011)), we also optimize over the target time T . The first variation with respect to T yields the simple relation

$$\frac{\partial \mathcal{L}}{\partial T} := \frac{1}{E_0} \frac{d}{dT} E(T) = 0 \quad (2.12)$$

provided \mathbf{u} is incompressible and satisfies the Navier-Stokes equations at $t = T$. Our algorithm then proceeds as follows. We first start with a suitable guess for the optimal initial condition, \mathbf{u}_0 and a target time T . We then time march our initial condition to time T using the Navier-Stokes equations and use $(\mathbf{u}/E_0 - \mathbf{v})|_{t=T} = 0$ to ‘initialise’ the adjoint equations which are then solved backwards in time to calculate \mathbf{v}_0 . This procedure ensures that all the variational equations are satisfied apart from (2.10) and (2.12). If the current value for \mathbf{u}_0 is optimal then (2.10) will be satisfied: on the other hand if (2.10) is not satisfied, it provides an estimate for the gradient $\delta \mathcal{L}/\delta \mathbf{u}_0$. Using this gradient we then use a method of steepest ascent to update our guess for \mathbf{u}_0 , while c is simultaneously calculated by ensuring that our new initial condition has an energy of E_0 . Once a new value of \mathbf{u}_0 is obtained, T is updated by integrating the Navier-Stokes equations forward in time using the updated \mathbf{u}_0 as an initial condition until a maximum value of $E(t)$ is reached. The time of this maximum is taken as the new value of T and (2.12) is then satisfied.

3. BF92 geometry

The underlying objective of this paper is to investigate how optimal initial conditions for energy growth some T later change as a function of E_0 . One specific issue is whether there is always an energy range below E_c where a NLOP is the optimal (a NLOP being an initial condition qualitatively different in structure and gain from the LOP). A second is whether $E_{fail} = E_c$ and a third is examining the form of the optimal as $E_0 \rightarrow E_c$ from above or below.

Results are first presented from a geometry studied previously in the linear regime ($E_0 \rightarrow 0$) in BF92: a periodic box with dimensions $L_x = 2\pi/0.49 = 13.66$, $L_y = 2$ and $L_z = 2\pi/1.9 = 3.31$ (or $4.08\pi \times 2 \times 1.05\pi$) with $Re = 1000$. A modified version of the Diablo CFD solver, (Taylor & Sarkar (2008)) which is spectral in x and z and finite difference in y , was used to solve the forward and adjoint equations using a resolution of $128 \times 256 \times 32$ in x , y and z respectively. For sufficiently low energies we found that the optimal perturbation was extremely similar to the LOP in both gain and structure and as result was named a ‘quasi linear optimal perturbation’ (QLOP). The QLOP achieved a maximum gain of approximately 1100 at $T = 125$ (in units of h/U). With increasing but still small E_0 , the gain and optimal time of the QLOP remains fairly constant as shown in figure 1(a). However, beyond a certain energy threshold, (approximately 2.3×10^{-6}) there is a sudden and large jump in the gain achievable, as shown in figure 1(b) (note the change of ordinate scale). In addition to the much higher gain at $E_0 = 2.3 \times 10^{-6}$, it is noticeable that the optimal time tends to very large values as E_0 approaches this transition energy from above. The initial conditions found by our algorithm there clearly evolve into a turbulent state given the much higher target-time kinetic energy values and the highly disordered endstate. This implies that $E_c \lesssim 2.3 \times 10^{-6}$ is the threshold energy for transition. To examine convergence, $\langle \delta \mathcal{L}/\delta \mathbf{u}_0, \delta \mathcal{L}/\delta \mathbf{u}_0 \rangle^{1/2}/G$ is plotted in figure 2 against iteration for $E_0 = 5.0 \times 10^{-7} < E_c$ and $E_0 = 5.0 \times 10^{-6} > E_c$.

For the smaller initial energy case (figure 2(a)) we see that after 10 iterations the gain has plateaued and that the value of the normalised gradient has dropped by 10 orders of magnitude, which suggests that the QLOP is converging well.

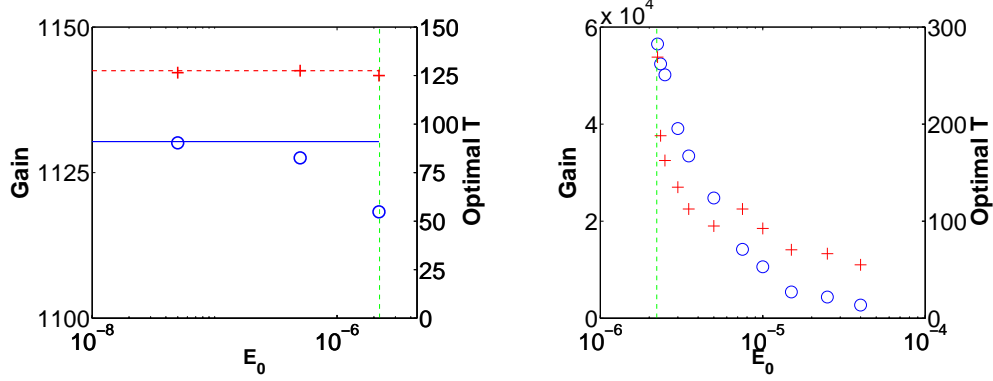


FIGURE 1. (a) Gain (blue circles) and associated optimal time (red crosses) against E_0 . $E_c \approx 2.3 \times 10^{-6}$ is marked by vertical green dashed line. LOP gain is the horizontal blue solid line, LOP optimal time is the horizontal red dashed line. (b) Gain (blue circles) and associated optimal time (red crosses) against E_0 for $E_0 > 2.3 \times 10^{-6}$.

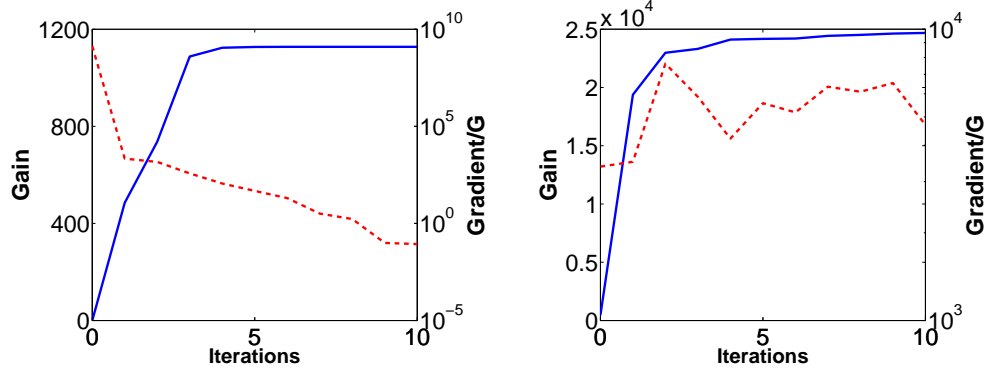


FIGURE 2. G (blue solid line) and $\langle \delta \mathcal{L} / \delta \mathbf{u}_0, \delta \mathcal{L} / \delta \mathbf{u}_0 \rangle^{1/2} / G$, (red dashed line) plotted against iteration for (a) $E_0 = 5.0 \times 10^{-7}$ (b) $E_0 = 5.0 \times 10^{-6}$. The QLOP presented in (a) appears to be converging well, whereas there is no convergence in (b).

Conversely, for the higher energy case (figure 2(b)) while the gain appears to plateau, the gradient is failing to decrease in size indicating the algorithm is not converging. In reality, because of the turbulent nature of the flow at time T we would not expect convergence to be possible, as a very small change in the initial condition is likely to produce a significant change in the final state. Despite this lack of convergence, the algorithm is successful in finding initial states which trigger turbulence when $E_0 > E_c$.

In the picture of PWK11, one unique initial condition - the minimal seed - should emerge as the limiting state for turbulence-triggering initial conditions as $E_0 \rightarrow E_c^+$. To examine the dynamical route states close to the minimal seed take to turbulent disorder, we have considered in detail a turbulent seed found at $E_0 = 2.3 \times 10^{-6}$ as it evolves in time. Figure 3(a) plots the kinetic energy and dissipation rate against time and in 3(b) the same quantities are plotted for the ‘rescaled’ turbulent seed whose initial energy

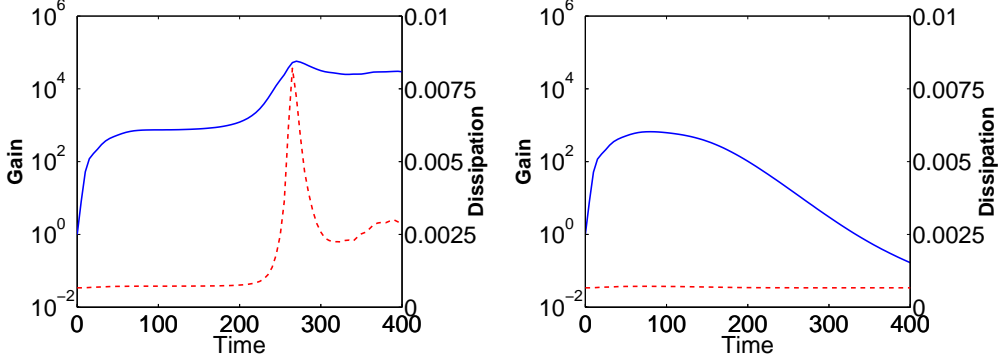


FIGURE 3. Gain (blue solid line) and dissipation (red dashed line) against time for (a) the turbulent seed at $E_0 = 2.3 \times 10^{-6}$ and (b) rescaled turbulent seed at $E_0 = 2.2 \times 10^{-6}$. Both initially behave similarly achieving a gain of approximately 1000. They maintain this energy level for an extended period of time, until $t \sim 150$. After this the turbulent seed has a noticeable spike in dissipation, indicating a transition to turbulence, whereas the rescaled turbulence seed decays away.

is $E_0 = 2.2 \times 10^{-6}$. The behaviours of the turbulent seed and rescaled turbulent seed are very similar up to $t \sim 75 h/U$. Beyond this time, however, the kinetic energies of the two initial perturbations begin to differ significantly, with the rescaled turbulent seed eventually decaying so the flow relaminarises whereas the turbulent seed triggers transition at $T \sim 270 h/U$. (Reassuringly, if the rescaled turbulent seed is used to initiate the optimizing procedure at $E_0 = 2.2 \times 10^{-6}$, the algorithm converges to the expected QLOP result.)

We observe in figure 3 that both flows spend an extended period of time at an intermediate (perturbation) energy level before going their separate ways. This is because both initial states are close to the edge (but on ‘opposite sides’) and spend some time tracking it while being gently repelled (in opposite directions). To confirm this, the turbulent seed and its rescaling can be used to refine the initial condition so that it stays nearer to the edge for longer (Itano & Toh (2001); Skufca *et al.* (2006); Schneider *et al.* (2007); Duguet *et al.* (2008)). In figure 4, this refinement is carried out to track the edge for $t = 400 h/U$ showing that the edge state (attracting state for edge-confined dynamics) has constant energy (consistent with the work of Schneider *et al.* (2008) who treat a PCF system $4\pi \times 2 \times 2\pi$ albeit at $Re = 400$ and find a steady edge state).

Figure 5 shows a side by side comparison of the contours of the perturbation streamwise velocity at $x = 0$ at four different times for the QLOP at $E_0 = 2.2 \times 10^{-6}$, the minimal seed at $E_0 = E_c$ (at least to the accuracy of figure 4) and the turbulent seed (which clearly is close to the minimal seed) at $E_c \lesssim E_0 = 2.3 \times 10^{-6}$. These plots demonstrate that while the minimal seed evolves towards the edge state, a small increase in its initial energy will lead to transition. As $E_0 \rightarrow E_c$ from above (below), the time to transition (relaminarisation) tends to ∞ due to the extra time needed to evolve upwards (downwards) in energy away from the edge. It is also clear that the QLOP is completely different from the minimal seed.

Finally it is worth examining the 3D structure of the time-evolving QLOP, the minimal seed and the turbulent seed just above the edge. In figure 6 we plot iso-contours of the streamwise velocity for times 0, 150, 250 and 350 (in unit of h/U). From the plots it is

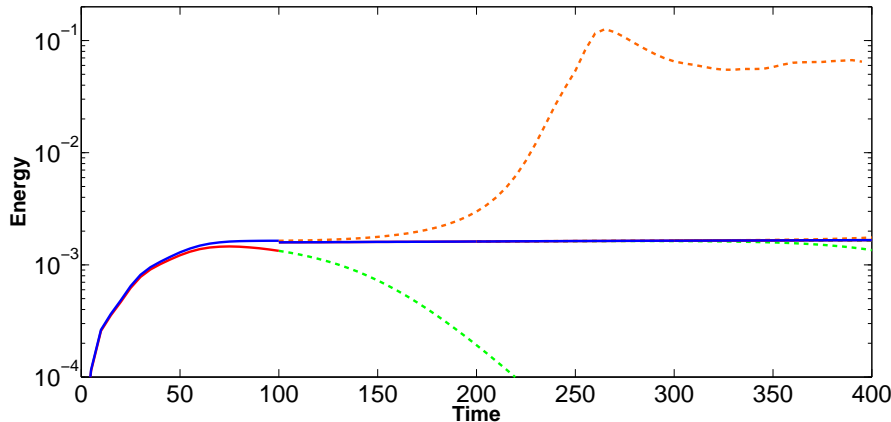


FIGURE 4. Perturbation energy against time for various initial states close to the edge. Upper bound of edge state blue, lower bound red. Every 100 time units, the edge state is rescaled to produce new upper and lower bounds. The minimal seed at E_c (blue line) stays on the edge (over this time period) and gets attracted to the edge state which emerges as having constant energy. The turbulent seed at $E_0 = 2.3 \times 10^{-6}$ is shown as the first blue/orange dashed line and the rescaled turbulent seed is the first red/green dashed line.

clear that the minimal seed is initially quite localized but quickly ‘unpacks’ itself into a series of a streamwise streaks. This unpacking process appears to be achieved by the well-known Orr mechanism followed by the lift-up mechanism. The minimal seed flow then remains in this configuration, whereas the streaks destabilise and there is transition to turbulence for the higher energy turbulent seed ‘above’ the edge.

To summarise, in this geometry and at this Re , it appears that a well-converged NLOP does not exist prior to our algorithm uncovering turbulence-triggering initial conditions at $E_0 = E_{fail}$. Our algorithm only fails to converge if there are turbulent seeds present so $E_{fail} \geq E_c$ and we find no evidence for inequality consistent with PWK11’s first conjecture. The minimal seed (as is apparent in figures 5 and 6) is qualitatively different from the QLOP, and so the optimals do not converge to the minimal seed as $E_0 \rightarrow E_c^-$, a clear counterexample to PWK11’s second conjecture.

4. M11 geometry

In this section we examine a second, larger geometry of dimensions $4\pi \times 2 \times 2\pi$ (essentially twice as wide as that in BF92) at a higher Reynolds number $Re = 1500$. We demonstrate in this geometry that now a NLOP exists at energies below E_c and investigate whether in the limit $E_0 \rightarrow E_c^-$ it converges to the minimal seed. Choosing the geometry and Reynolds number used by M11 has the added benefit that we can compare our results to those obtained using an entirely different functional. M11 optimized the total dissipation over a long time interval rather than the energy gain achieved at a specific target time. We find a critical energy value $E_c = 3.3 \times 10^{-7}$, plotted in figures 7 (a) and (b), which agrees well with M11, who find $3 \times 10^{-7} < E_c < 4 \times 10^{-7}$ (see their figure 1). Note ϵ_0 in M11 is E_0 here as $\| \cdot \|_E$ in their equation (1) is strictly a kinetic norm with a $\frac{1}{2}$ included (Monokrousos, personal communication). Our calculated time for transition at $E_0 = 4.0 \times 10^{-7}$ is approximately 200 not too dissimilar from the time of 150 in M11. This suggests that the particular choice of optimizing functional is not important for the calculation of a minimal seed (or more accurately to lose convergence),

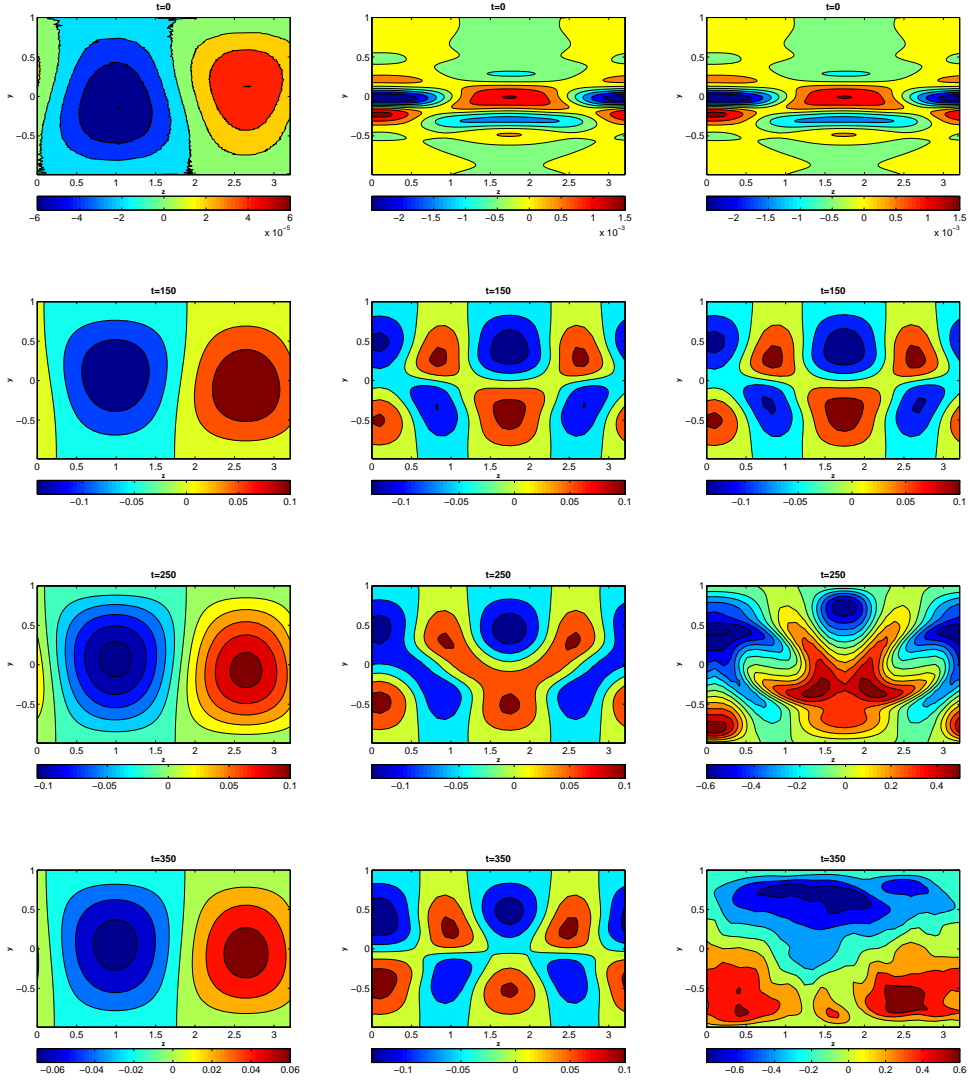


FIGURE 5. Contours of streamwise velocity u at times 0, 150, 250, 350 for QLOP (left), minimal seed (centre) with $E_0 = E_c$ and turbulent seed (right) for $E_0 = 2.3 \times 10^{-6} \gtrsim E_c$. Contour levels are: going down the left column (min,spacing,max) $=(-6, 2, 6) \times 10^{-5}$, $(-0.1, 0.05, 0.1)$, $(-0.1, 0.02, 0.1)$ and $(-0.06, 0.02, 0.06)$; going down the centre (min,spacing,max) $=(-2, 0.5, 1.5) \times 10^{-3}$ and $(-0.1, 0.05, 0.1)$ subsequently; going down the right column (min,spacing,max) $=(-2, 0.5, 1.5) \times 10^{-3}$, $(-0.1, 0.05, 0.1)$, $(-0.6, 0.1, 0.5)$ and $(-0.6, 0.2, 0.6)$.

provided the functional attains heightened values for turbulent flows (as discussed in PWK11).

Figure 7(a) indicates that three energy regimes exist in this geometry rather than the two in BF92. As before, below a certain initial energy value, a QLOP is selected and above a critical energy E_c initial conditions significantly different from the QLOP trigger turbulence. Between these two energy regions, however, there now exists a range of initial

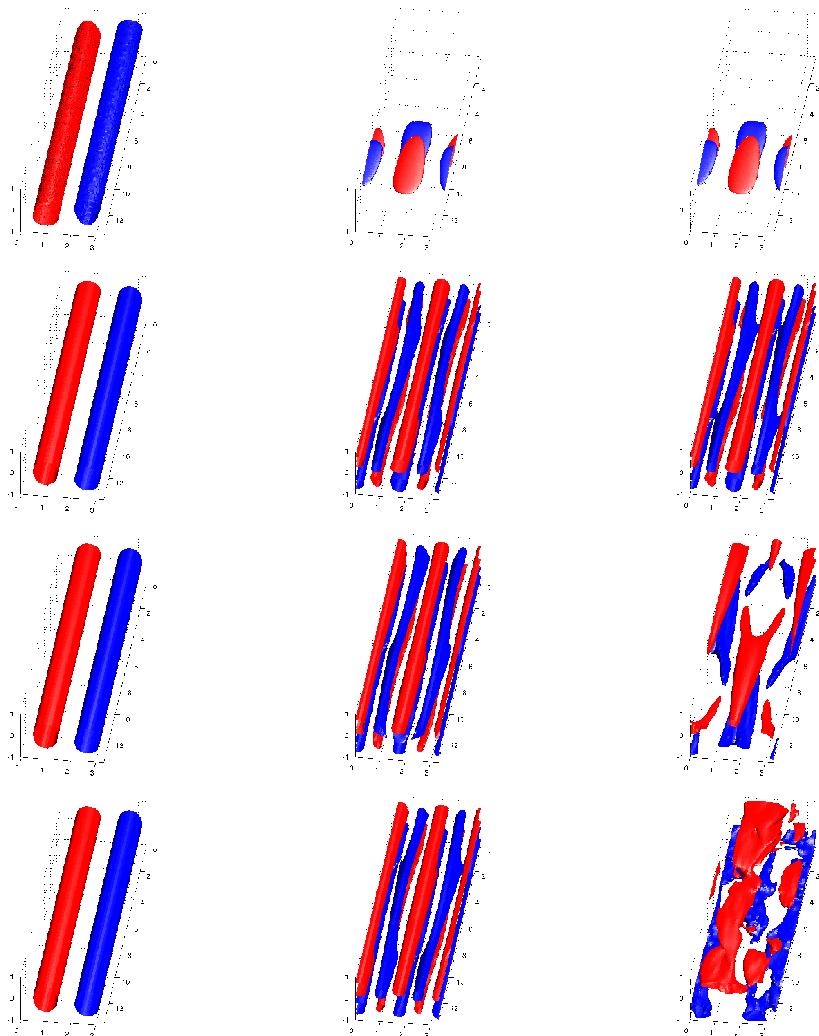


FIGURE 6. Iso surfaces of streamwise velocity u , at 60% of maximum and minimum values, for the QLOP at $E_0 = 2.2 \times 10^{-6}$ (left), the minimal seed (centre) and a turbulent seed above the edge at $E_0 = 2.3 \times 10^{-6}$ (right), at times 0, 150, 250, 350.

energies where our algorithm generates an initial condition different from the QLOP (in the sense that it appears to have a qualitatively different spatial structure) - see figure 8. Using the nomenclature described in the introduction, we call this qualitatively different optimal perturbation a NLOP after Pringle & Kerswell (2010) and PWK11. Figure 9 contrasts the convergence for the NLOP with the non-convergence in the turbulent seed region $E_0 > E_c$. Only five points are plotted in figure 9 as for additional iterations (however small we made our step size in the direction of the gradient) it was not possible to find a new \mathbf{u}_0 with a gain that improved on the previous iteration.

As a consequence of the kinetic energy gains of the NLOP and QLOP becoming very similar around $E_0 = 1.0 \times 10^{-7}$, the cross-over between the NLOP and QLOP is hard to pinpoint. If the NLOP is used to initialise the algorithm for energies slightly above E_c , the algorithm is found to converge to an initial condition very similar to the NLOP. In fact, the algorithm started with random noise will still sometimes converge to the NLOP

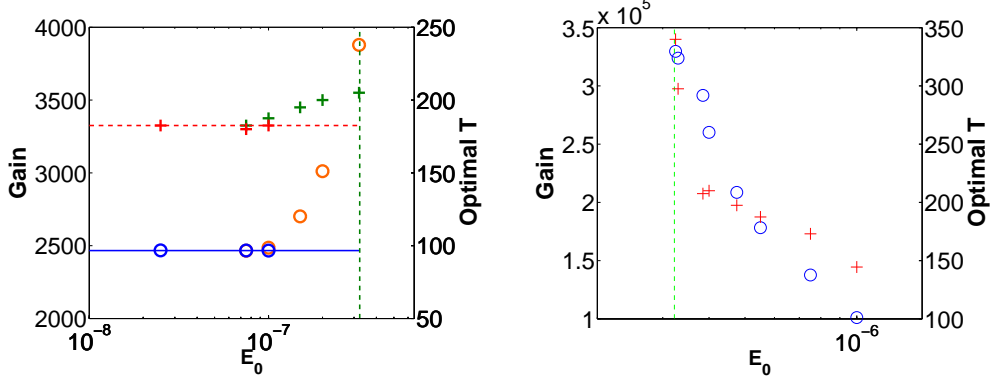


FIGURE 7. (a) Gain, $E(T)/E(0)$, of QLOP (blue circles) and NLOP (orange circles) and associated optimal time of QLOP (red crosses) and NLOP (green crosses), T , against E_0 . E_c is marked by vertical green dashed line. LOP gain horizontal blue solid line, LOP optimal time horizontal red dashed line. (b) Gain, $E(T)/E(0)$, (blue circles) and associated optimal time (red crosses), T , against E_0 . E_c is marked by vertical green dashed line.

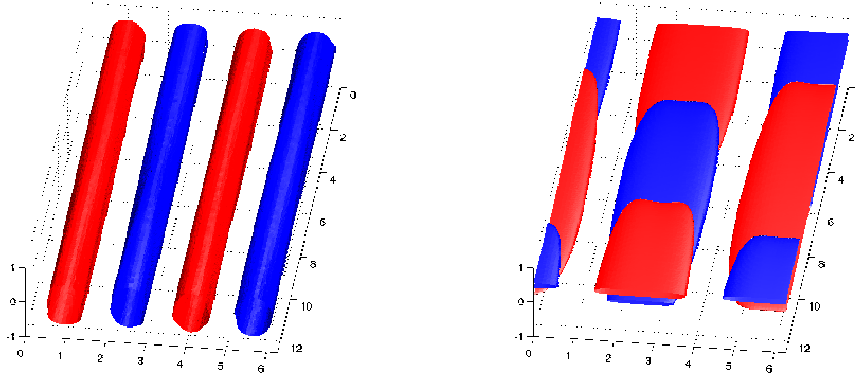


FIGURE 8. Iso surfaces of streamwise velocity u , at 60% of maximum and minimum values, for (a) QLOP at $E_0 = 5.0 \times 10^{-8}$ and (b) NLOP at $E_0 = 3.2 \times 10^{-7}$. It is clear that the NLOP is distinct from the QLOP.

for values of E_0 twice as large as E_c . As a consequence, approaching E_c from above proved a better strategy. Random noise was used at $E_0 \sim 2.5 \times 10^{-6} \approx 7.5E_c$ to find a turbulent seed and then this was used sequentially to initiate the algorithm as E_0 was gradually decreased. This experience clearly emphasizes the main hazard of nonlinear optimisation: it is easy to get stuck near local maxima. Although not a cure, an obvious strategy to reduce this possibility is to look for robustness of result over a suite of initial conditions.

Figure 7 also indicates that the turbulent seeds show the same trend, as in the BF92 geometry, with regards to the optimal target time, namely that it increases drastically as $E_0 \rightarrow E_c^+$. We conclude that the turbulent seeds remain near the edge for an even greater period of time than the turbulent seeds in the BF92 geometry. This may be because they are closer to the edge and/or that the edge is less repelling. As before, we have traced the edge up to $t = 400 h/U$ using a slightly rescaled turbulent seed to find a similar

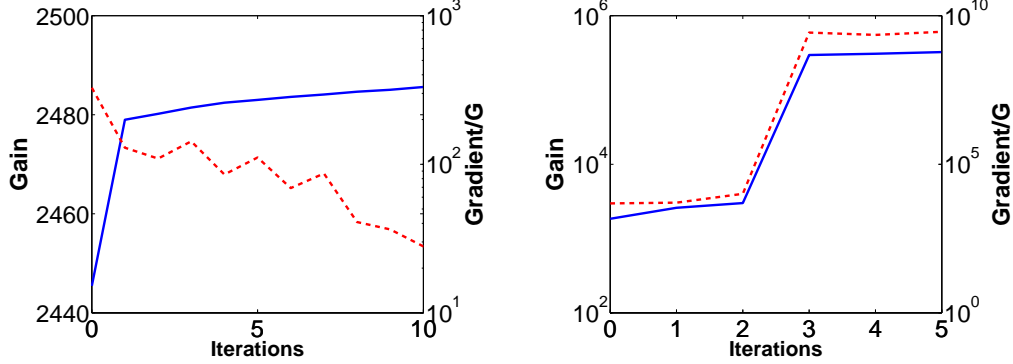


FIGURE 9. G (blue solid line) and $\langle \delta\mathcal{L}/\delta\mathbf{u}_0, \delta\mathcal{L}/\delta\mathbf{u}_0 \rangle^{\frac{1}{2}}/G$ (red dashed line) plotted against iteration for (left) $E_0 = 1.0 \times 10^{-7}$ and (right) $E_0 = 3.3 \times 10^{-7}$. The NLOP (left) appears to be converging well, whereas the calculation which throws up turbulent seeds does not.

plot to figure 4 (not shown). A comparison of cross sectional streamwise velocities for the NLOP at $E_0 = 3.2 \times 10^{-7}$, the minimal seed and the turbulent seed at 3.3×10^{-7} in figure 10 again emphasizes their different temporal evolutions despite being so close energetically. Also interestingly, the NLOP is localised in the cross-stream direction and is not dissimilar from the minimal seed although they are clearly not the same. This is made obvious by comparing their streamwise structure: see the top row of figure 11.

Figure 11 also shows how the NLOP unpacks into a series of streamwise streaks. An examination of the early time suggests that it is a combination of the Orr and lift-up mechanisms (as discussed in PWK11) that is responsible for the localized flow unpacking into streamwise streaks. The minimal and turbulent seeds also unpack in the streamwise and cross-stream direction producing streamwise streaks which are still spanwise localised. If there is sufficient energy in these streaks they are unstable (the turbulent seed) otherwise not (the minimal seed). By comparing the isosurface of the QLOP at time zero (figure 8) and the isosurfaces depicting the time evolution of the NLOP it is clear that the NLOP evolves into a structure which is very similar to the QLOP. This suggests that while at early time there exists a distinct NLOP structure, which is able to extract enhanced gain from the base flow by ‘unpacking’, it later exploits the same ‘lift-up’ mechanism as the QLOP at intermediate times.

It is significant that the minimal and turbulent seeds are spanwise-localised (at least until the turbulence is reached) in this 2π wide geometry and not in the 1.05π wide geometry of BF92. Of course the higher Re must be a contributory factor but the spanwise dimension does seem important. Pringle & Kerswell (2010) originally found an azimuthally-localised (and radially-localised) NLOP in a short pipe where one could talk about a ‘spanwise’ (azimuthal) lengthscale of 2π (radii or half-channel heights). The emergence of a NLOP in the wider geometry is also noteworthy. The LOP, and by definition QLOP, are global periodic states which are largely insensitive to the geometry, whereas the gathering evidence is that the NLOP is an attempt by the fluid to localise in order to maximise the energy gain for given *global* kinetic energy. As a result, the general trend should be for the energy cross-over from QLOP to NLOP to *decrease* with increasing domain size. Clearly this cross-over is above E_c for the BF92 geometry at $Re = 1000$ and below E_c for the M11 geometry at $Re = 1500$.

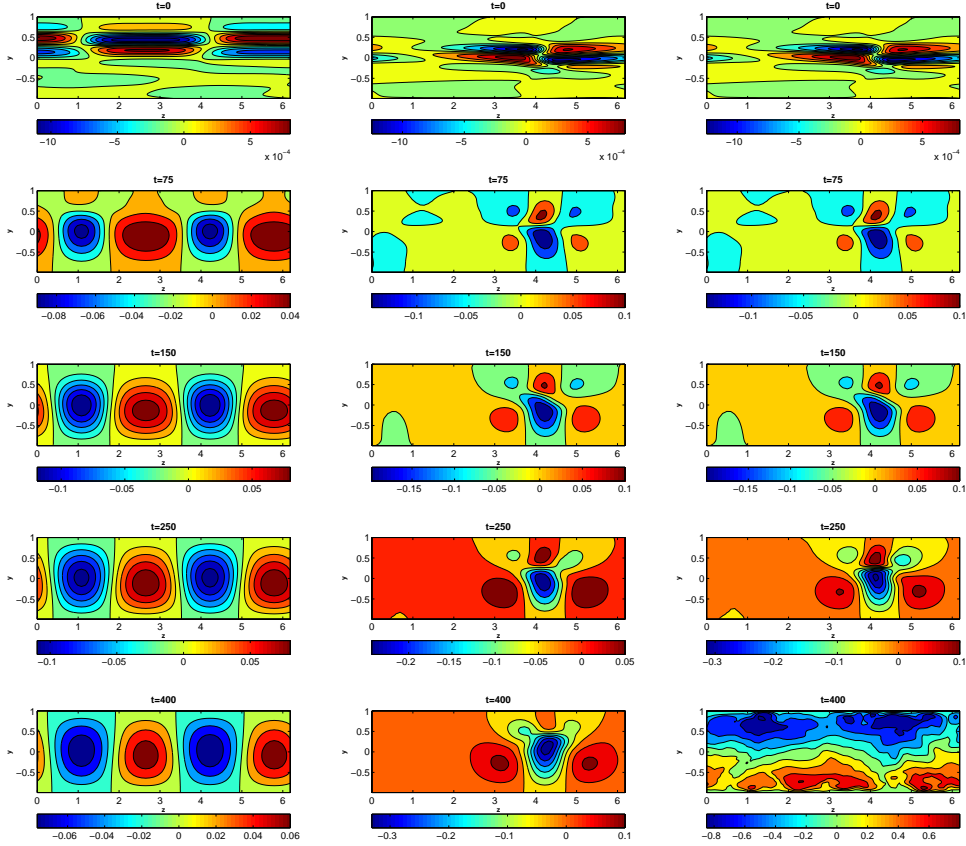


FIGURE 10. Contours of streamwise velocity u for NLOP $E_0 = 3.2 \times 10^{-7}$ (left), approximated minimal seed and turbulent seed at $E_0 = 3.3 \times 10^{-7}$ (right), at times 0, 75, 150, 250 and 400. At intermediate times, the minimal seed flow on the edge and that initiated from the turbulent seed remain relatively similar. Contour levels are: going down the left column (min,spacing,max) $=(-10, 2, 8) \times 10^{-4}$, $(-0.08, 0.02, 0.04)$, $(-0.1, 0.02, 0.08)$, $(-0.1, 0.02, 0.08)$, and $(-0.06, 0.02, 0.06)$; going down the centre (min,spacing,max) $=(-10, 2, 8) \times 10^{-4}$, $(-0.1, 0.05, 0.1)$, $(-0.15, 0.05, 0.1)$, $(-0.2, 0.05, 0.05)$ and $(-0.3, 0.05, 0.1)$; going down the right column (min,spacing,max) $=(-10, 2, 8) \times 10^{-4}$, $(-0.1, 0.05, 0.1)$, $(-0.15, 0.05, 0.1)$, $(-0.3, 0.05, 0.1)$ and $(-0.8, 0.2, 0.8)$.

The evolution shown in the right column of figure 11 looks very similar to that shown in figure 4 of M11 (albeit at a slightly different initial energy) indicating that we have generated an approximation to the same (presumably unique) minimal seed. This is further supported by the aforementioned correspondence in their and our estimates for E_c . Beyond validating each others results (which is important for nonlinear optimisation problems), this points to an insensitivity in the choice of the functional to be maximised for finding the minimal seed. There is one proviso, of course, that the functional must be selected so that it detects turbulent flows by assuming large values as discussed in PWK11.

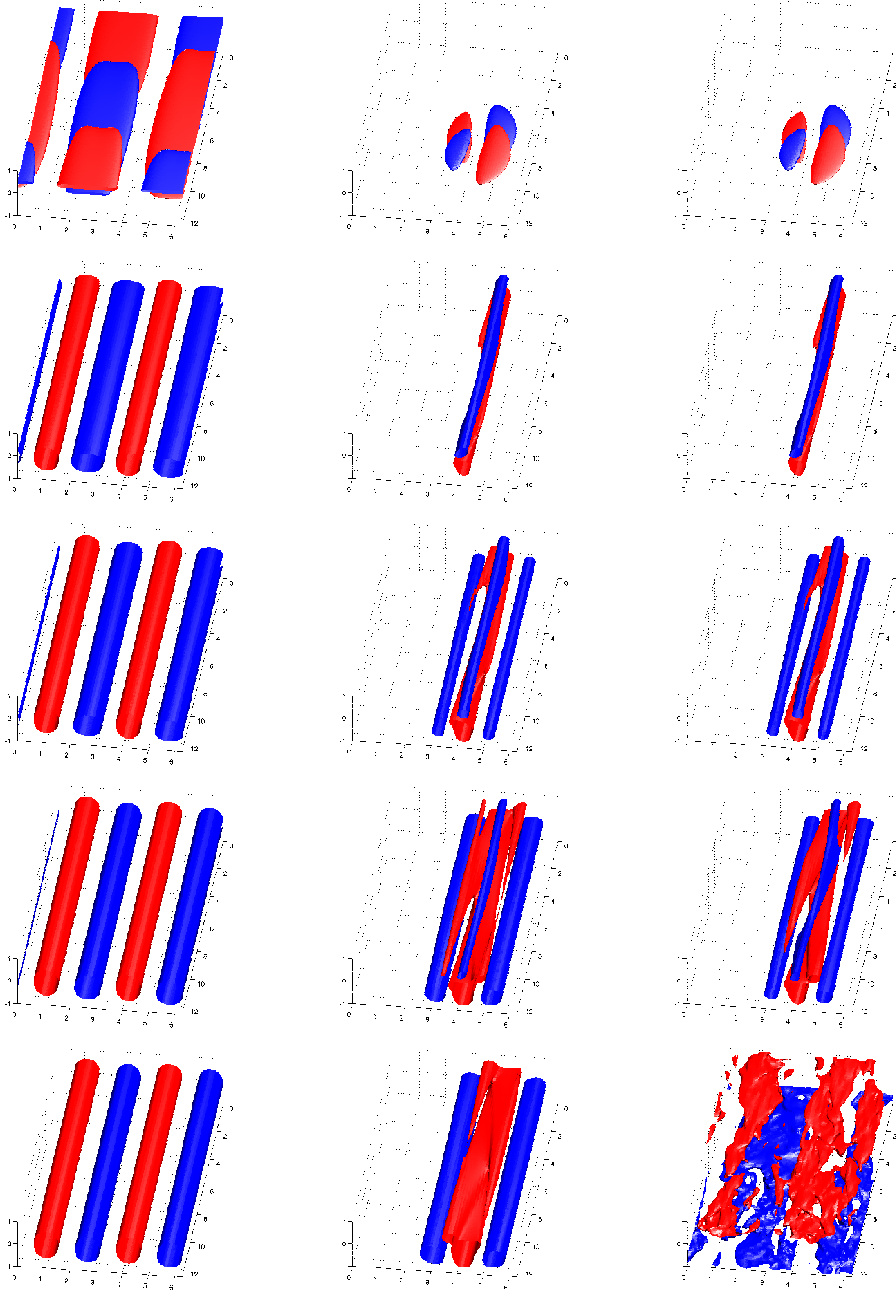


FIGURE 11. Iso surfaces of streamwise velocity u , at 60% of maximum and minimum value, for NLOP $E_0 = 3.2 \times 10^{-7}$ (left), approximated minimal seed (centre) and turbulent seed at $E_0 = 3.3 \times 10^{-7}$ (right), at times 0, 75, 150, 250 and 400. The minimal and turbulent seeds are initially localized but quickly unpack into streamwise streaks, which are stable for the minimal seed but unstable for the turbulent seed ultimately leading to breakdown.

5. Discussion

In this paper, we have sought the disturbance to plane Couette flow of a given finite kinetic energy E_0 which will experience the largest subsequent energy gain $G = E(T)/E_0$ where the time of maximum gain T is an *output* of our variational formulation. Two geometry- Re situations have been considered: $(L_x \times L_y \times L_z, Re) = (4.08\pi \times 2 \times 1.05\pi, 1000)$ as it was used for the original calculations of linear optimals in Butler & Farrell (1992) and $(4\pi \times 2 \times 2\pi, 1500)$ for which analogous calculations have recently been performed optimising the total dissipation over a specified period in Monokrousos *et al.* (2011). Our results can be summarised as follows.

(a) A nonlinear optimal (NLOP) distinct from the ‘nonlinearised’ linear optimal (QLOP) exists only in the wider geometry at the Re considered.

(b) In both situations, there exists an energy E_{fail} beyond which the variational algorithm no longer converges due to the existence of turbulence-triggering initial conditions. This means $E_{fail} \geq E_c$, the energy above which turbulence can be triggered. PWK11’s first conjecture is that $E_{fail} = E_c$ if the energy hypersurface is sufficiently sampled and we find nothing to contradict this.

(c) The QLOP or NLOP are not found to converge to the minimal seed (the disturbance of lowest energy which can trigger turbulence) as $E_0 \rightarrow E_c^-$ contradicting PWK11’s second conjecture.

(d) The failure of our variational algorithm to optimise energy gain appears to give the same estimate for E_c and the minimal seed as optimising the total dissipation over a long time period Monokrousos *et al.* (2011). This confirms the ‘robustness of failure’ of the variational approach discussed by PWK11 providing the functional to be optimised assumes large values for turbulent flows.

The underlying motivation for all these types of optimising calculations is the hope that the ‘optimal’ perturbation at $E_0 < E_c$ for an appropriately selected functional bears some relation to disturbances of lowest energy which actually trigger turbulence. By optimising the energy gain, PWK11 found this was at least approximately the case for their pipe flow set-up. Here though, this is clearly not true in either PCF situation studied. Ironically, however, the variational procedure *does* identify these turbulence-triggering disturbances and the critical energy for transition E_c but only indirectly by failing to converge. Importantly, we have also found evidence that this revealing failure to converge is insensitive to the exact functional selected providing the functional takes on heightened values for turbulent flows as argued in PWK11. Taken together, the variational approach adopted here seems to offer a fairly robust new theoretical tool to examine the *nonlinear* stability of fluid flows.

Many applications suggest themselves, but here we just note one - assessing the stabilizing or destabilizing influence of applied flow perturbations or controls. Normally, this would be attempted either by investigating the linearised operator around the base (laminar) flow or by carrying out exhaustive numerical simulations. The current work suggests a third way where the movement (in phase space) of the laminar-turbulent boundary towards (destabilisation) or away (stabilisation) from the base flow is investigated. We hope soon to report on some calculations along these lines.

Acknowledgements: We would like to thank A. Monokrousos and D. Henningson for helping us make contact with their work (M11). SMER would like to thank S. Dalziel and A. Holyoake for their invaluable help with computational issues and G. Chandler for insightful discussions. He is supported by a doctoral training award from EPSRC, and would like to acknowledge the Entente cordiale scholarship program for support during the production of this manuscript. This work was performed using the Darwin Supercomputer of the University of Cambridge High Performance Computing Service (<http://www.hpc.cam.ac.uk/>), provided by Dell Inc. using Strategic Research Infrastructure Funding from the Higher Education Funding Council for England. The research activity of CPC is supported by EPSRC Research Grant EP/H050310/1 “AIM (Advanced Instability Methods) for industry”. CPC would also like to acknowledge the generous hospitality of the Hydrodynamics Laboratory (LadHyX) École Polytechnique/CNRS during the production of this manuscript.

REFERENCES

- BOTTIN, S. & CHATE, H. 1998 Statistical Analysis of the Transition to Turbulence in Plane Couette Flow. *Eur. Phys. J. B* **6** (1), 143–155.
- BUTLER, K. M. & FARRELL, B. F. 1992 3-Dimensional Optimal Perturbations in Viscous Shear-Flow. *Phys. Fluids A* **4** (8), 1637–1650.
- CHERUBINI, S., PALMA, P. DE, ROBINET, J. CH. & BOTTARO, A. 2010 Rapid Path to Transition via Nonlinear Localized Optimal Perturbations in a Boundary-Layer Flow. *Phys. Rev. E* **82**, 066302.
- DUGUET, Y., WILLIS, A. P. & KERSWELL, R. R. 2008 Transition in Pipe Flow: the Saddle Structure on the Boundary of Turbulence. *J. Fluid Mech.* **613**, 255–274.
- GUSTAVSSON, L. H. 1991 Energy Growth of 3-Dimensional Disturbances in Plane Poiseuille Flow. *J. Fluid Mech.* **224**, 241–260.
- ITANO, T. & TOH, S. 2001 The Dynamics of Bursting Process in Wall Turbulence. *J. Phys. Soc. Japan* **70**, 703–716.
- MONOKROUSOS, A., BOTTARO, A., BRANDT, L., VITA, A. DI & HENNINGSON, D. S. 2011 Nonequilibrium Thermodynamics and the Optimal Path to Turbulence in Shear Flows. *Phys. Rev. Lett.* **106** (13), 134502.
- PRINGLE, C. C. T. & KERSWELL, R. R. 2010 Using Nonlinear Transient Growth to Construct the Minimal Seed for Shear Flow Turbulence. *Phys. Rev. Lett.* **105** (15), 154502.
- PRINGLE, C. C. T., WILLIS, A. P. & KERSWELL, R. R. 2011 Minimal Seeds for Shear Flow Turbulence: Using Nonlinear Transient Growth to Touch the Edge of Chaos arXiv:1109.2459v1.
- REDDY, S. C. & HENNINGSON, D. S. 1993 Energy Growth in Viscous Channel Flows. *J. Fluid Mech* **252**, 209–238.
- ROMANOV, V. A. 1973 Stability of Plane-Parallel Couette Flow. *Functional Anal. Applics.* **7**, 137–146.
- SCHMID, P. J. 2007 Nonmodel stability theory. *Ann. Rev. Fluid Mech.* **39**, 129–162.
- SCHNEIDER, T. M., ECKHARDT, B. & YORKE, J. A. 2007 Turbulence Transition and the Edge of Chaos in Pipe Flow. *Phys. Rev. Lett.* **99**, 034502.
- SCHNEIDER, T. M., GIBSON, J. F., LAGHA, M., LILLO, F. DE & ECKHARDT, B. 2008 Laminar-Turbulent boundary in plane Couette flow. *Phys. Rev. E* **78**, 037301.
- SKUFCA, J. D., YORKE, J. A. & ECKHARDT, B. 2006 Edge of Chaos in a Parallel Shear Flow. *Phys. Rev. Lett.* **96**, 174101.
- TAYLOR, J. R. & SARKAR, S. 2008 Stratification Effects in a Bottom Ekman Layer. *J. Phys. Oceanogr.* **38**, 2535–2555.